L Aho-Mantila et al.

Assessment of SOLPS5.0 Divertor Solutions with Drifts and Currents against L-mode Experiments in ASDEX Upgrade and JET

Assessment of SOLPS5.0 Divertor Solutions with Drifts and Currents against L-mode Experiments in ASDEX Upgrade and JET

L. Aho-Mantila[1], S. Potzel[2], D.P. Coster[2], M. Wischmeier[2], M. Brix[3], R. Fischer[2], S. Marsen[4], A. Meigs[3], H.W. Müller[2], A. Scarabosio[2], M.F. Stamp[3], S. Brezinsek[5], the ASDEX Upgrade Team and the JET Contributors‡[6]

[1] VTT Technical Research Centre of Finland, P.O.Box 1000, FI-02044 VTT, Finland
[2] Max-Planck-Institut für Plasmaphysik, D-85748 Garching, Germany
[3] CCFE, Culham Science Centre, Abingdon, UK
[4] Max-Planck-Institut für Plasmaphysik, Teilinstitut Greifswald, Germany
[5] Institut für Energie- und Klimaforschung - Plasmaphysik, Forschungszentrum Jülich, Germany
[6] EUROfusion Consortium, JET, Culham Science Centre, Abingdon, OX14 3DB, UK

E-mail: `leena.aho-mantila@vtt.fi`

Abstract. The divertor solutions obtained with the plasma edge modelling tool SOLPS5.0 are discussed. The code results are benchmarked against carefully analysed L-mode discharges at various density levels and with and without impurity seeding in the full-metal tokamaks ASDEX Upgrade and JET. The role of the cross-field drifts and currents in the solutions is analysed in detail, and the improvements achieved by fully activating the drift and current terms in view of matching the experimental signals are addressed. The persisting discrepancies are discussed.

‡ See the Appendix of F. Romanelli et al., Proceedings of the 25th IAEA Fusion Energy Conference 2014, Saint Petersburg, Russia

1. Introduction

Edge fluid codes have been developed to calculate the properties of the scrape-off layer (SOL) and divertor plasma, in order to understand in detail the exhaust processes and the ways to control them. Such understanding is required to assess the feasibility of current power exhaust scenarios in future reactors, a task which would be significantly easier if the codes could be shown to possess some predictive power. A major limitation is the lack of first principle models for the radial transport, which currently is treated with a set of prescribed transport coefficients, required as an input from the modeller. In recent years, the code solutions have been put through detailed benchmarking tests against experimental measurements, in which the ability of the codes to calculate the divertor conditions for given radial transport assumptions deduced from the upstream conditions has been assessed in comparison to detailed profile measurements at the targets [1, 2, 3, 4, 5]. In most cases, the tests have revealed significant discrepancies between the simulations and experiments, particularly regarding the processes leading to divertor detachment and divertor in–out asymmetries, see e.g. [1, 2, 3]. This raises a concern that fundamental deficiencies exist either in the commonly applied input assumptions or in our models for the exhaust processes.

The most common edge fluid code packages in use (e.g. SOLPS [6], EDGE2D-Eirene [7, 8, 9], UEDGE [10], SOLEDGE2D [11], SONIC [12]) share similar features: they are based on 2D multifluid codes, which can be run coupled to a Monte Carlo neutrals code, or even to a Monte Carlo impurity code (SONIC). None of the codes calculate turbulent transport from first principles, but the typical approach is to fit the radial transport levels according to experimental (profile) measurements. Strong poloidal variations in turbulent transport have been considered as an explanation for part of the discrepancies observed when comparing the simulations to the experiments [13, 14]. Further transport mechanisms discussed are the cross-field drifts. Both experimental and analytic considerations have suggested that cross-field drifts ($\mathbf{E} \times \mathbf{B}$ and diamagnetic) could significantly modify the power and particle sharing between the divertor legs, therefore influencing the power load on the targets and the access to the detached divertor regime required in high-power devices like ITER [15, 16, 17, 18]. Drift models have been included in most of the 2D fluid codes, which calculate self-consistently the potential distribution and the various divertor plasma-neutral interactions. However, the activation of the drift terms introduces numerical (and sometimes physical) convergence problems, which can only be overcome by running the code with a small timestep. This leads to such long computational times, that attempts to benchmark drift simulations (in particular for complex plasmas with impurities) have been limited in the past. Furthermore, in those attempts which have been made, an unambiguous assessment of drift effects has been challenging due to lack of global consistency with the diagnostic measurements, see e.g. [19, 1].

In this paper, we present benchmarking work dedicated to assessing the influence of drifts on the SOL simulations. The validity of the solutions is first assessed in comparison to experimental data obtained from two full-metal devices: ASDEX Upgrade and JET. The comparisons are carried out for diagnostic measurements at the low-field-side midplane and in the two active divertor legs in a lower-single-null configuration in low-confinement mode (L-mode). For validation of the divertor models an extensive diagnostic coverage is used, including measurements both in the divertor volume and at the divertor targets. For the first time, quantitative comparisons are made with the divertor density measurements via Stark broadening

in ASDEX Upgrade (see also [20] and the presentations related to [21, 22], as well as recent results in [23]). The results are then compared to the corresponding divertor solutions obtained without any drift terms activated (but with the calculation of currents), and the possible improvements obtained with the activation of drift terms are discussed. In order to better understand the role of drifts on the target conditions, we investigate the impact of the various drift terms on the power and particle flux asymmetries at the divertor entrance as well as on the transport processes taking place inside the two divertor legs.

The drifts inside the divertor are likely to be sensitive to the divertor regime (e.g. detached compared to attached divertor) and to the local temperature and density gradients, whereas it is unclear how much the divertor conditions influence the drifts in the main SOL. To assess the role of drifts in various divertor regimes, two different exhaust scenarios are considered. First, the role of drifts is analysed as a function of increasing upstream density (n_{sep}), which in the L-mode discharges is achieved by D-fuelling alone. With increasing n_{sep} the target ion fluxes are first measured to increase, reaching maximum values, after which a "roll-over" occurs and the ion fluxes begin to reduce. This roll-over of the ion fluxes is considered a typical indication of divertor detachment [2, 24]. Second, radiative L-mode divertor plasmas are addressed, in which controlled levels of N-seeding are injected into the plasma in order to radiate large fractions of the total heating power. This leads to significant changes in the target power loads. Both the SOL and the divertor plasmas can be expected to behave differently between these two L-mode scenarios. In the first, high-density scenario, the increase of n_{sep} leads to a higher upstream collisionality and reduces the temperature upstream (typical for L-mode), such that relatively small parallel temperature gradients are obtained along the field lines. In the low-density seeding scenario, the effects of N-seeding are much more localized in the divertor, leading at high radiated power fractions to strong local gradients near the divertor entrance, but not necessarily strong changes in the upstream conditions compared to the unseeded reference discharge (provided that the seeding levels are not high enough to lead to strong radiation on closed field lines, which often makes N-seeded L-mode plasmas unstable). The steepness of the parallel gradients is further influenced by the device size and divertor geometry, which differ between JET and ASDEX Upgrade.

The paper is organized as follows. Section 2 describes the characterization experiments performed in the two devices. Section 3 describes the modelling approach. In Section 4, we present a detailed benchmarking of the divertor solutions against the diagnostic measurements in the experiments. In Section 5, we analyse the physics behind the observations made in the experiments and in the simulations, focusing particularly on the role of drifts and currents. In Section 6, the remaining discrepancies are discussed and, finally, a summary and conclusions are presented in Section 7.

2. Experiments

The experiments used in this paper for benchmarking the SOL simulations have been performed in the ASDEX Upgrade and JET tokamaks. The ASDEX Upgrade tokamak has a major radius of 1.6 m, and a fully W-coated first wall and divertor was used in the time of these experiments. The JET tokamak has a major radius of 3 m, and an ITER-like wall with Be in the main chamber and W in the divertor. The benefit of using two full-metal devices is that the intrinsic impurity levels can be kept low, which simplifies the species mix which needs to be taken into account when modelling

these devices [21]. In both devices, a lower-single-null (LSN) configuration optimised for diagnostic measurements was used for all discharges, and the discharges were all performed in L-mode. In JET, the discharges have been performed with the outer strike point positioned on the horizontal outer target, whereas the ASDEX Upgrade discharges used a vertical target configuration with the so-called edge-optimized shape (EOC). These configurations, as well as the locations of the relevant divertor diagnostics, are shown in Figures 3, 4 and 9.

In both devices, as similar as possible reference discharges were first carried out at a relatively low main plasma density, see Tab. 1. For ASDEX Upgrade, similar low-density discharges have been modelled earlier with SOLPS5.0 to study the effects of the magnetic field reversal on the divertor conditions [4], and the results of that validation work are used as a starting point for the present studies. In the present discharges, a higher plasma current ($I_{\mathrm{p}} = 1.0$ MA instead of 0.8 MA) has been used, and the external heating had to be reduced to $P_{\mathrm{ECRH}} = 0.4$ MW to avoid transition to H-mode. The toroidal magnetic field was 2.5 T in both devices, and a plasma current of 2.5 MA was used at JET. At low enough line-averaged density ($\overline{\mathrm{n}}_{\mathrm{e}}$), the outer divertor can be kept in a low-recycling regime in both ASDEX Upgrade and JET, and strong plasma-neutral interaction (e.g. charge exchange, volume recombination) can be avoided. This allows us to better focus on the validation of the transport physics in the simulations, in comparison to plasmas with strong plasma–neutral interaction.

In order to assess the role of drifts in plasmas with varying collisionality and parallel temperature gradients, we have studied two different variations to the above reference conditions. First, the discharge density is increased to $\overline{\mathrm{n}}_{\mathrm{e}} = 5.7 \times 10^{19}$ m^{-3} by increasing the D fuelling rate in ASDEX Upgrade. As $\mathrm{n}_{\mathrm{sep}}$ is increased, the divertor plasma goes through 3 different states of divertor detachment, labelled as the *onset of detachment*, the *fluctuating detachment state*, and the *complete detachment state* [24], see Fig. 1. It is not expected that the drifts would play a major role in complete detachment in L-mode, because the high upstream density tends to correspond to low upstream temperature and correspondingly high collisionality and weak electric fields in the SOL. Therefore, we focus in the present work on the power exhaust characteristics in the first two detachment states. At $\overline{\mathrm{n}}_{\mathrm{e}} = 4.0 \times 10^{19}$ m^{-3} (reference case), the inner divertor is at the onset of detachment in ASDEX Upgrade, whereas at $\overline{\mathrm{n}}_{\mathrm{e}} = 5.7 \times 10^{19}$ m^{-3}, maximum ion fluxes are obtained in the inner divertor (in Fig. 1, the roll-over point is at slightly (4%) lower $\overline{\mathrm{n}}_{\mathrm{e}} = 5.5 \times 10^{19}$ m^{-3}, which could be due to the fast density ramp-up compared to the steady-state conditions studied in the present paper, or due to other small differences in machine conditions or diagnostic measurement uncertainties).

In addition to the upstream density variation, a power exhaust scenario with N seeding is analysed in both devices. The corresponding scans in the N-seeding level, Γ_{N}, have been performed and analysed in a previous publication [21]. In the present paper, we analyse the steady-state conditions obtained with a fixed Γ_{N} in each device. These levels correspond to the maximum radiated power fractions, $\mathrm{f}_{\mathrm{rad}} = P_{\mathrm{rad,tot}}/P_{\mathrm{tot}} \sim 60\%$, obtained in the experiments: here, $P_{\mathrm{rad,tot}}$ is the total radiated power (with negligible core radiated power fraction [25]) and P_{tot} is the total heating power. In these discharges, $\overline{\mathrm{n}}_{\mathrm{e}}$ is kept constant, which limits the plasma density also in the divertor, leading to a smaller neutral pressure and weaker plasma-neutral interaction compared to the high-density discharge.

All discharges presented in this paper have been carefully diagnosed in view of validating the divertor plasma models. The main diagnostics used for this purpose
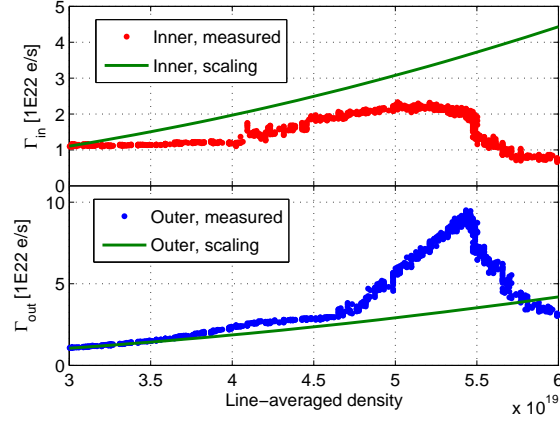
Figure 1. Evolution of the ion fluxes at the two divertor targets of ASDEX Upgrade as a function of line-averaged density. The data is taken from discharge #27100 [24]. Similar to [24], the green lines show the simple two-point model scalings of the ion fluxes ($\propto \overline{n}_e{}^2$), normalised to the measured ion fluxes at low density ($n_{sep} \sim 3 \times 10^{19}$ m^{-3}), separately for each target.

Discharge	Device	Type	$\overline{n}_e$	P_{tot}	Γ_N
#27688	AUG	high density	5.7E19 m^{-3}	1.3 MW	-
#27691	AUG	reference	4.0E19 m^{-3}	1.0 MW	-
#28818	AUG	seeding	4.0E19 m^{-3}	1.0 MW	3.4E21 e/s
#82291	JET	reference	2.7E19 m^{-3}	2.7 MW	-
#82295	JET	seeding	2.7E19 m^{-3}	2.7 MW	7.5E21 e/s

Table 1. Summary of the main discharges analysed in this paper. The total power, P_{tot}, is the sum of the auxiliary heating power and the ohmic power.

are the spectroscopic systems and the Langmuir probes at the two targets, see Fig. 3 and Fig. 4. The primary diagnostic measurements used for the benchmarking are the target ion fluxes, temperatures and Balmer line emissions. In the exhaust regimes (high density and seeded plasmas), the temperature measurements obtained by the Langmuir probes are considered too uncertain due to the low temperature values and possibly high impurity concentrations, and are left outside the scope of this paper. Care is taken when analysing those Balmer lines that might overlap strong impurity lines in the N-seeded discharges (such as the D$_\delta$ line at 410.2 nm, which has neighbouring NIII lines at 409.8 nm and 410.3 nm).

3. SOLPS5.0 simulations

The experiments have been modelled using the SOLPS5.0 code package [6]. SOLPS5.0 is a code package built around the 2D B2.5 plasma multifluid code. It includes an optional coupling to the 3D Monte Carlo neutrals code Eirene, which is often used when modelling present-day devices. The 1999 version of Eirene is used in all simulations presented in this paper. A typical computational region includes the SOL field lines connecting to the target plates, the divertor and the private flux regions, as well as the mantle region with closed field lines.

The modelling of the two devices discussed here uses the same physics ingredients

for both devices when possible. In all of the so-called drift simulations, cross-field drifts ($\mathbf{E} \times \mathbf{B}$, diamagnetic) and currents are activated in the whole computational region (the drifts have been slowly ramped up with a simulation time step varying between 10^{-6} s and 10^{-5} s). The simulated species include the D main plasma species, accounting for the neutral and molecular physics as described in [3], as well as the seeded impurity N, accounting for its ionization and volume recombination. The line radiation of both species is calculated using the cross-section data from ADAS. The default assumption is that D and N are fully recycled at the wall elements, excluding the pumping surfaces described below. The assumption for N is in line with recent ASDEX Upgrade experiments, which showed a saturation of the N content of the divertor surfaces within a single L-mode discharge [26, 27], and the assumption for D follows conventional approximations, as the effective recycling coefficient cannot be deduced for each individual experiment but is expected to be close to 1. The radial transport properties are identical for all ions and described by radially varying diffusion coefficients. The radially varying heat conduction coefficients account for the anomalous heat transport, separately for the ions and the electrons. In both devices, a small level of ballooning of the transport coefficients ($\propto B^{-1}$) is assumed in the poloidal direction, similar to [1]. The level is chosen such as to maintain a simultaneous agreement with the LFS measurements both at the upstream and at the target locations, and it is observed to have a negligible impact on the divertor asymmetries compared to the drift effects discussed in Sec. 5 (stronger ballooning with $B^{-\alpha}$ dependence yields too peaked target profiles, which could be avoided by using a dependence on the poloidal angle as in [28], but is left outside the scope of the present work).

The wall configuration and computational mesh for ASDEX Upgrade are similar to what has been used in earlier benchmarking work [4]. In the present simulations, all wall elements are specified to be W, but with no sputtering yield (due to the negligible measured core radiated fractions in the experiments, no W impurities are followed in the simulations). Subdivertor structures have been included in order to limit the conductance of neutrals between the divertor and the pumping region, and pumping surfaces at realistic locations with various pumping albedos are specified in the ASDEX Upgrade simulations. These structures and albedos allow to match typical pressure drops in a free molecular regime with and without the presence of a (low density) plasma [29]. In the JET simulations, the wall elements are specified to be Be in the main chamber and W in the divertor, with no sputtering of either material. A similar approach to modelling the subdivertor region as in ASDEX Upgrade has not been attempted in the present work for JET, which has a smaller coverage of neutral pressure gauges in the subdivertor region. Instead, pumping surfaces have been specified as shown in Figure 4, with a pumping albedo of 95% (fraction of reflected flux from incident flux), which is specified to match the experimental D fuelling level in the low-density reference discharge.

As discussed already in the introduction, the simulations require assumptions to be made on the radial transport in the plasma edge. In the present work, the radial transport properties are adjusted to match the measured upstream profiles in the unseeded discharges, see Fig. 2. The assumptions are not, however, fully constrained by the upstream profiles, as it is well known that the measured profiles near the separatrix and in the SOL have (i) a scatter of data points, see Fig. 2, allowing for a large number of possible solutions (i.e. combinations of transport assumptions and upstream input parameters) that match the measurements, and (ii) an uncertainty in
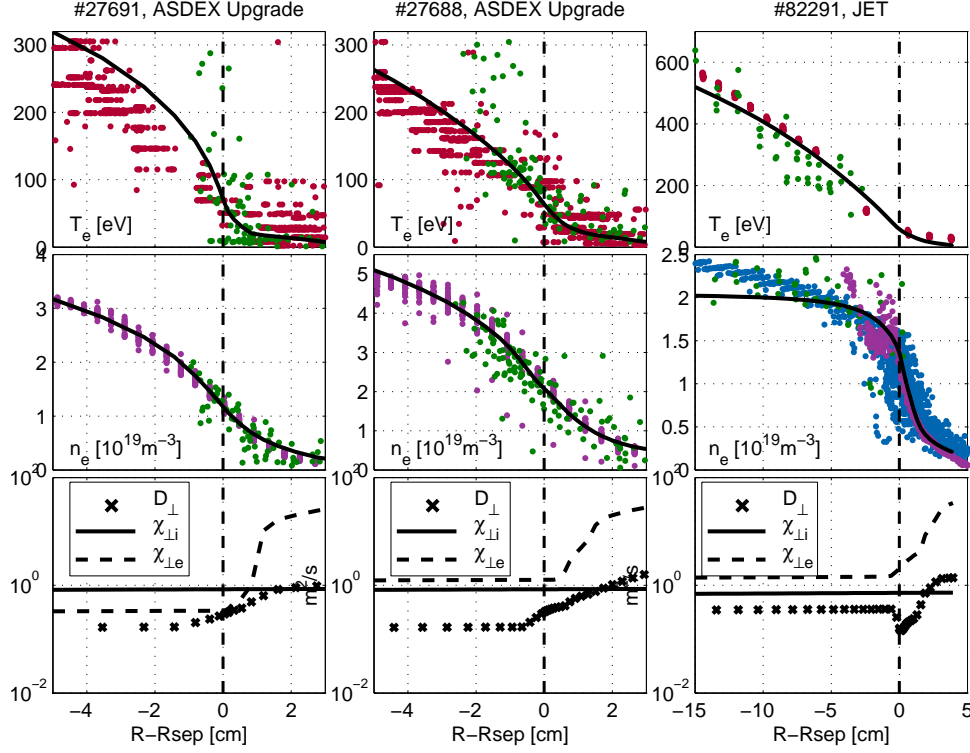
Figure 2. Measured and modelled profiles of T_e (top row), n_e (middle row), and the specified transport coefficients ($D_\perp$, $\chi_{\perp,i}$, $\chi_{\perp,e}$, bottom row) at the outer midplane. The temperature measurements are obtained from ECE (red) and Thomson scattering (green), and the density measurements are from IDA (purple, AUG), Li-beam (purple, JET), reflectometry (blue, JET) and Thomson scattering (green). The IDA profile in ASDEX Upgrade is obtained as a combination of the Li-beam and the laser diagnostics. Based on the uncertainties in the radial positioning of the diagnostic data and the separatrix location, as well as the uncertainty range of the measurements, n_{sep} can vary between 0.8–$1.6\times10^{19}\mathrm{m}^{-3}$ (#27691) and 1.5–$2.8\times10^{19}\mathrm{m}^{-3}$ (#27688) in ASDEX Upgrade, and between 0.7–$1.7\times10^{19}\mathrm{m}^{-3}$ in JET.

the radial position, such that solutions with a higher and lower separatrix density, n_{sep}, are possible. The separatrix position is uncertain by 0.5 cm in ASDEX Upgrade and by 1.0 cm in JET, and similar radial shifts can exist for the mapping of the diagnostics with respect to each other. Therefore, the outer target profiles are taken as a further guidance for the selection of n_{sep} and the transport coefficients (in other words, as close as possible agreement with the low-field-side measurements is sought for, both upstream and at the target). This "tuning" of the input parameters is carried out in the simulations with activated drifts and currents for all the unseeded discharges presented in this paper. No further adjustments are made when N impurities are seeded into these discharges, as the assumption is that the upstream conditions are largely unchanged by the seeding in L-mode, and the observed changes in the target conditions are due to SOL impurity radiation and its effects on the volumetric processes and drifts. In all modelled cases, no further tuning of the input parameters is made to match the conditions in the inner divertor or at other poloidal locations in
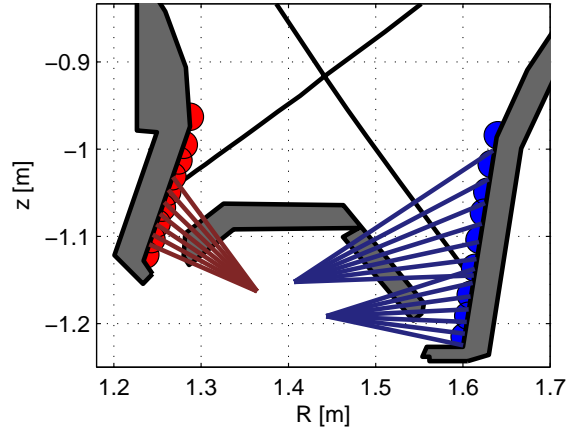
Figure 3. Configuration of divertor diagnostics used in the ASDEX Upgrade discharges (apart from the measurements carried out with the FVS spectrometer, which are shown in Fig. 9). The solid lines show the lines-of-sight of the EVS spectrometer, and the solid circles show the locations of the flush-mounted Langmuir probes at the inner and outer target, red and blue colours, respectively. All the EVS LOS were looking at the gaps between the tiles, which should minimize measurements of reflected emission originating from other regions in the plasma.

the SOL (for recent work with such poloidal variations in the transport assumptions, see [23]). No further tuning of the input parameters is made for the solutions without activated drift terms.

4. Benchmarking the modelled divertor power and particle distributions

The drift simulations are assessed in the present paper in view of the modelled divertor power and particle distributions, including the possible in–out asymmetries between the two divertor legs. We first analyse the asymmetries by performing comparisons between the measured and modelled plasma conditions at the two targets. This includes the Langmuir probe data as well as spectroscopic measurements of various Balmer lines on poloidally distributed lines-of-sight. We then proceed to assessing in more detail the detachment process in the inner divertor of ASDEX Upgrade, by performing comparisons with D_δ Balmer line and density measurements carried out with a high-resolution spectrometer along lines-of-sight distributed in the inner divertor volume.

4.1. Target conditions and asymmetries

We begin by analysing the so-called reference discharges, which were carried out at low $\overline{n}_e$ and which best allow to validate the transport models in the simulations, see Table 1. Figure 5 shows the modelled and measured target conditions in these discharges, measured by the flush-mounted Langmuir probes (see Figs. 3 and 4 for the diagnostic positions). Looking at the experimental measurements alone, one notices a large asymmetry between the two divertor targets in both devices. In ASDEX Upgrade, the outer divertor is in a low-recycling regime, with a relatively hot peak temperature ($\sim$ 40 eV). The inner divertor is much cooler, and the measured peak
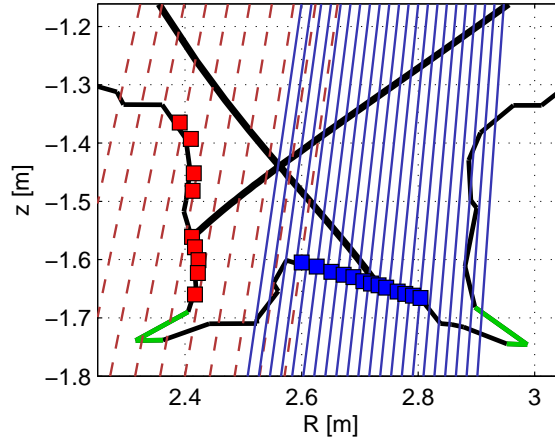
Figure 4. Configuration of divertor diagnostics used in the JET discharges. The dashed red lines show the LOS of the KS3 spectrometer (inner divertor), the solid blue lines show the LOS of the KT3 spectrometer (outer divertor). The solid squares show the flush-mounted Langmuir probes at the inner and outer targets, red and blue colours, respectively. The wall geometry is the one used in the simulations, and the modelled pumping surfaces are indicated with the green colour.

ion fluxes are 50% lower at the inner target compared to the outer target. In JET, a strong asymmetry is observed in the divertor temperature similar to the ASDEX Upgrade conditions, but the peak ion fluxes are at least a factor of 2 higher at the inner target compared to the outer target. Therefore, experimentally, a difference exists in the measured ion flux asymmetry between the two experiments, whereas the T_e asymmetry is similar between the two devices.

In addition to the experimental measurements, Fig. 5 shows two SOLPS5.0 solutions for both devices. The first solution is obtained using the default simulation settings (explained in detail in Section 3) with all drift and current terms activated (referred to as solutions *with drifts*), whereas the second solution is obtained by deactivating the drift terms (but with currents still activated, referred to as solutions *without drifts*). Without drifts, the modelling yields very symmetric conditions for the two targets in both devices, failing to reproduce the experimental observations of strongly asymmetric T_e distribution. With the activation of drift terms, the desired in–out asymmetries in the divertor temperature are obtained. The ion flux asymmetry is, however, reproduced only in the case of JET. In ASDEX Upgrade, the modelled ion fluxes exceed the measured ion fluxes at the inner target by a factor of 3 when drifts are activated in the simulations. Recalling Fig. 1, the experimental measurements for ASDEX Upgrade indicate the onset of detachment at the inner target at this upstream density level (corresponding to $\overline{n}_e \sim 4 \times 10^{19}$ m^{-3}), which results in smaller measured ion fluxes than what a simple 2-point model scaling would yield. In the simulations, the inner target is still attached, which results in an in–out asymmetry in Γ_{tot} that is opposite to the experiments when drifts are activated. In JET, the inner divertor is not yet detaching in the low-density experiment, and the modelled high-recycling inner divertor conditions are in much better agreement with the measurements. Possible reasons for the different inner divertor regimes measured between the two devices include the differing inner divertor geometries and connection lengths to the X-point,
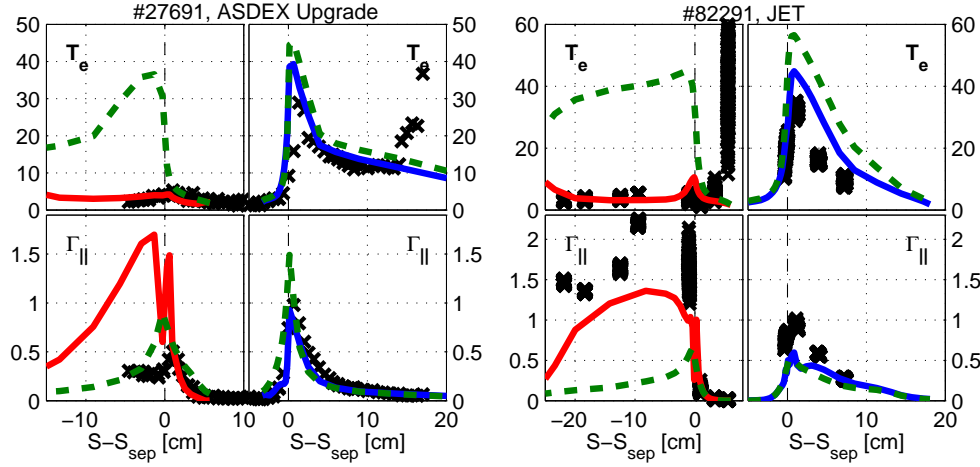
Figure 5. Comparisons between the modelled and measured target electron temperatures, T_e [eV], and ion fluxes, $\Gamma_\parallel$ [10^{24} m^{-2}s^{-1}], top and bottom row, respectively. The results are shown for the ASDEX Upgrade discharge #27691 and for the JET discharge #82291 (the so-called low-density reference discharges). For both discharges, the inner divertor comparisons are shown on the left side, and the outer divertor comparisons are on the right side. The Langmuir probe measurements are drawn with the black crosses, the simulations with drifts with the solid lines (red and blue for inner and outer divertor, respectively), and the simulations without drifts (but with currents activated) with the dashed green lines.

see Figs. 3 and 4.

In Fig. 6 comparisons are made between the modelled and measured Balmer line emissions. The measurements in ASDEX Upgrade were carried out using a spectrometer which covers the 410 nm D_δ line, the 434 nm D_γ line and the 486 nm D_β line, see Fig. 3 for LOS distribution. In JET, two different spectrometers were used for the inner and outer divertor, yielding either the 656 nm D_α line and the 434 nm D_γ line, or the 410 nm D_δ line and the 434 nm D_γ line, respectively. The LOS distributions are shown in Fig. 4. Comparisons with the 434 nm D_γ line are shown on the bottom row of Fig. 6 for each target, whereas on the top row a higher Balmer line is preferably drawn, except for the outer target of JET, for which only the lower Balmer line 410 nm D_δ was available. In ASDEX Upgrade, the modelling results lie generally below the measurement results, and the modelled peak emissions are a factor of 2-3 below the measured peak emissions. Such discrepancies are outside the uncertainty range of the intensity calibration (20%). On the contrary, a satisfactory agreement is obtained between the modelled and measured Balmer line emissions in JET, when comparing only the simulations with drifts to the experiments. In this case, the profiles along the two targets are largely reproduced, apart from the region near R=2.4 m in the inner divertor. This location is close to the strike point and to the protrusion of the inner target towards the plasma at z=-1.5 m, see Fig. 4. It is possible that either some of the emission is shadowed and the spectrometer cannot measure accurately at this location, or the emission is sensitive to the position of the inner strike point. Both of these effects are not necessarily correctly modelled due to the uncertainty of the inner strike point position (a few cm). The simulations without
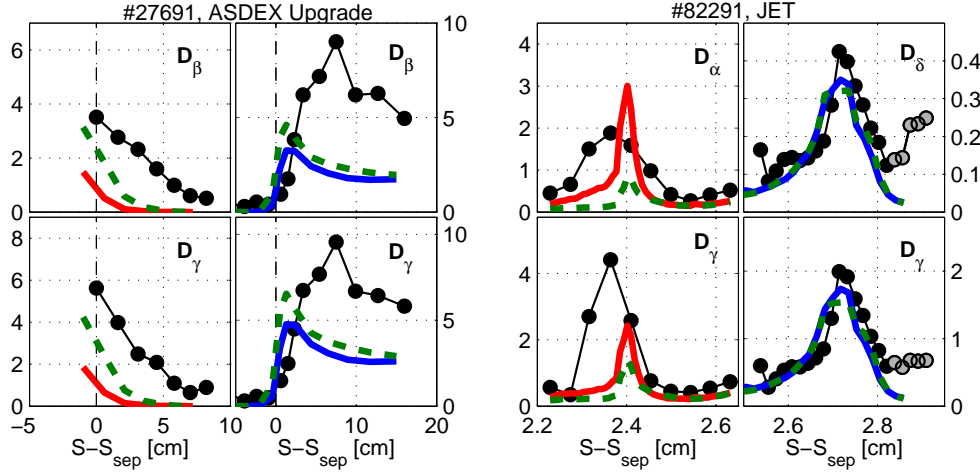
Figure 6. Comparisons between the modelled and measured Balmer line emissions, D_α [10^{20}Ph/sr/m^2/s], D_β [10^{18}Ph/sr/m^2/s] and D_γ [10^{17}Ph/sr/m^2/s] (see annotations in the individual plots). The results are shown for the ASDEX Upgrade discharge #27691 and for the JET discharge #82291 (the so-called low-density reference discharges). For both discharges, the inner divertor comparisons are shown on the left side, and the outer divertor comparisons are on the right side. The spectroscopic measurements are drawn with the black circles, the simulations with drifts with the solid lines (red and blue for inner and outer divertor, respectively), and the simulations without drifts with the dashed green lines. The grey circles indicate those measurements which are most likely to include some reflected light, representing an upper boundary for the experimental conditions.

drifts yield a less satisfactory agreement with the inner target measurements.

We turn next to the validation of the simulations when a high-recycling regime is obtained at the outer target. Fig. 7 shows the comparisons between the modelled and the measured ion saturation currents and the 434 nm D_γ line in the N-seeded discharges, recall Table 1. At $f_{rad} = 60\%$, the simulations yield a high-recycling outer divertor regime in both devices, similar to the experiments. As in the experiments, the modelled outer target ion fluxes are higher with seeding than in the absence of seeding, in both devices. Nevertheless, both the total and the peak modelled outer target ion fluxes are factors of 2–3 below the measured values in both devices, both with and without drifts activated. These discrepancies are not significantly larger than the (up to a factor of 2) discrepancies observed when modelling the unseeded reference discharges. In ASDEX Upgrade, the inner divertor is in the detached regime in the experiment, similar to the unseeded reference discharge, but the detachment is not reproduced in the modelling even at the modelled high radiated power fraction of 60% (both the measured ion fluxes and the measured neutral emission are not reproduced by the modelling). In JET, the inner divertor is in the experiment in the high-recycling regime at $f_{rad} = 60\%$, but the modelled peak ion flux is a factor of 2 smaller than the measured peak ion flux, similar to the discrepancy observed when modelling the unseeded reference discharge. In ASDEX Upgrade, the discrepancies with Balmer line emission become larger with seeding compared to the unseeded discharge in the PFR of both targets, but the discrepancy in the outer divertor SOL region remains as in the unseeded discharges, a factor of 2–3. In JET, a satisfactory agreement is observed
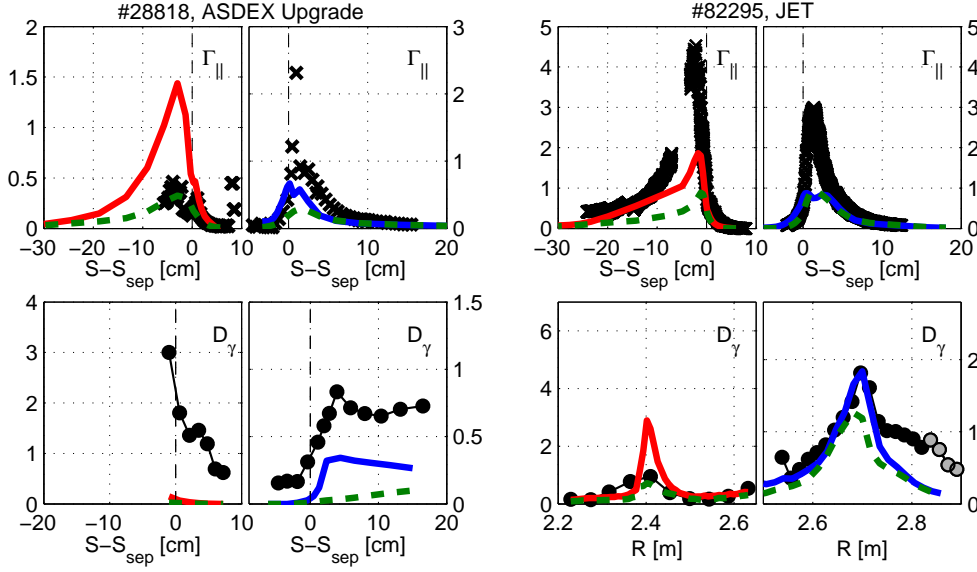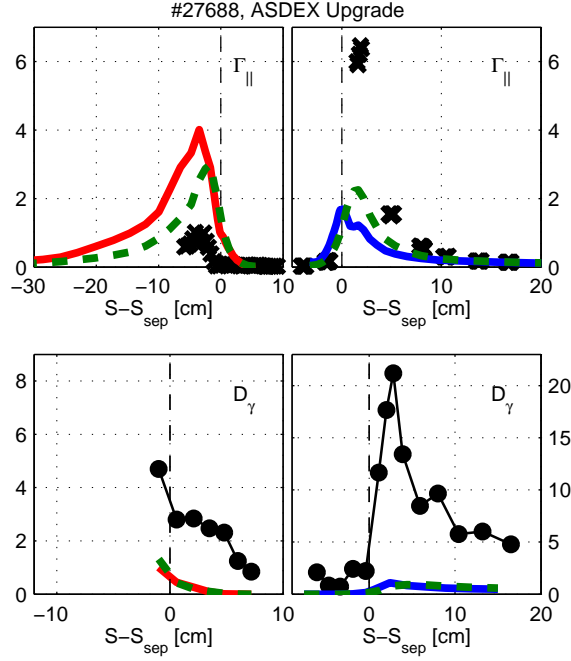
Figure 7. Comparisons between the modelled and measured target ion fluxes, $\Gamma_{\parallel}$ [10^{24} m^{-2}s^{-1}], and Balmer line emissions, D_{γ} [10^{18}Ph/sr/m^2/s], top and bottom row, respectively. The results are shown for the N-seeded ASDEX Upgrade low-density discharge #28818 and the N-seeded JET low-density discharge #82295. Figure details as in 5 and 6.

between the modelled and the measured Balmer line emissions in the outer divertor, similar to the reference discharges, and the most significant discrepancies are observed at the inner target, near the strike point. Again, this could at least partially be related to detailed geometry effects, which cannot be taken into account due to the limited resolution of the calculated magnetic equilibrium.

Fig. 8 shows the same comparisons for the high-density ASDEX Upgrade discharge #27688. In this discharge the upstream density is measured to be a factor of 2 higher compared to the low-density reference discharge, and the measured total ion flux to the inner target is similarly a factor of 2 higher than in the reference discharge. As in the experiments, the simulations for the high-density discharge yield a similar factor of 2 increase of the peak inner target ion flux compared to the low-density discharge. Therefore, similar to the comparisons at low n_{sep}, a factor of 3 discrepancy is obtained between the measured and the modelled inner target ion flux at high n_{sep}. The discrepancy between the measured and the modelled Balmer line emission is of the same order of magnitude as in the low-density discharge. The agreement between the modelled and the measured conditions at the outer target is, however, significantly worse at high n_{sep} compared to low n_{sep}. The simulations underestimate the peak ion fluxes by a factor of 6, and the modelled peak Balmer line emission is a factor of 10 smaller than in the experiments, both with and without drifts. The discrepancies are in the same direction as in the N-seeded discharges, i.e. the ion fluxes and neutral emission are underestimated in the high-recycling regime, but the level of discrepancy is much higher at high n_{sep} (without seeding) compared to low n_{sep} (with seeding).

The observations from these target comparisons can be summarized as follows (all observations are specific to L-mode). At low n_{sep} and without a significant level

Figure 8. Comparisons between modelled and measured target ion fluxes, $\Gamma_\parallel$ [10^{24} m^{-2}s^{-1}], and Balmer line emissions, D_γ [10^{18}Ph/sr/m^2/s], top and bottom row, respectively. The results are shown for the unseeded ASDEX Upgrade high-density discharge #27688. Figure details as in 5 and 6.

of seeded impurities, the measured strong temperature asymmetry between the two targets can be reproduced by the modelling for both JET and ASDEX Upgrade, provided that the drifts are activated in the simulations (see similar observations of drift effects in [18, 4]). Simultaneously, the emission from neutrals can be either satisfactorily reproduced (JET) or it can be a factor of 2–3 off (ASDEX Upgrade). Similar to earlier results [2, 19], the inner target ion fluxes are overestimated by the modelling when the experimental measurements indicate a detached inner divertor regime in ASDEX Upgrade. This conclusion can be drawn in the present work both at low and high n_{sep} and with and without a significant fraction of N impurities in the plasma, i.e., for both low and high radiated power fractions. When the measurements indicate a high-recycling regime in either the outer or the inner divertor, a smaller Γ_{pk} is modelled than what is measured in both JET and ASDEX Upgrade. The discrepancy is observed to be significantly larger at high n_{sep} than at low n_{sep}. Based on the comparisons shown here, the discrepancy between the modelled and the measured Γ_{pk} and neutral emission can be quantitatively much larger in the high-recycling conditions (outer divertor) than in the detached conditions (inner divertor).

4.2. Inner divertor detachment in ASDEX Upgrade

Although discrepancies between modelling and experiments were observed at both targets, and the largest discrepancies were obtained in high-recycling conditions at the outer target, the inability to reproduce the detached state of the inner divertor
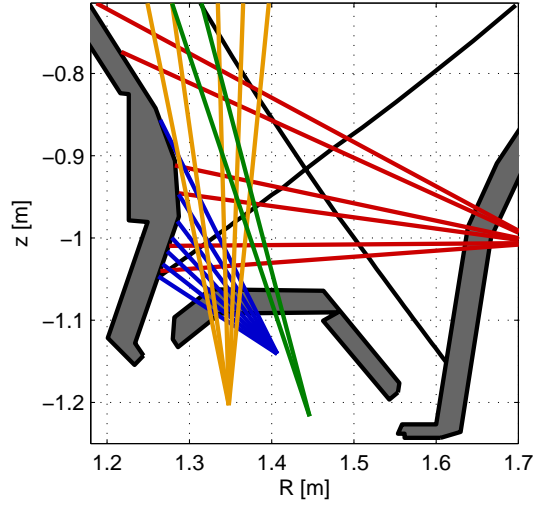
Figure 9. Setup of LOS used in the high-resolution FVS spectrometer for analysing the Stark broadening of the Balmer lines in the ASDEX Upgrade discharges.

has been a large concern in earlier ASDEX Upgrade studies [14, 19]. To investigate the inner divertor conditions further, an enhanced spectroscopic viewing configuration has been developed, with LOS covering the inner divertor volume both in radial and in poloidal directions [30]. A similar configuration was used to study the inner divertor conditions in the ASDEX Upgrade experiments analysed in the present paper, see Fig. 9. These LOS were connected to a spectrometer which measured the 410 nm Balmer line D_δ with a high wavelength resolution, enabling the determination of the Stark broadening profile and separation of the D_δ peak from the neighbouring impurity lines. The Stark broadening is sensitive to the local electron density, and analysis of the Balmer lines is used to determine the density in the inner divertor volume [30]. In the context of the present work, we have developed a similar synthetic diagnostic in SOLPS5.0, which calculates the inner divertor n_e corresponding to the diagnostic measurement, by utilizing the modelled densities and line emissions along the specified LOS.

Figs. 10 and 11 show the comparisons between the modelled and measured n_e and D_δ. For analysing the reference low-density conditions (discharge #27691), the measurements were obtained under similar conditions in a diagnostic repeat discharge #27981. For analysing the high-density conditions (discharge #27688), the measurements were obtained at a relevant time point in a density ramp-up discharge #27100 [24] (the relevant time point was chosen by comparing the measured divertor conditions between the two discharges, not $\overline{n}_e$). In the low-density N-seeding discharge #28818 the Stark broadening measurements were performed successfully during the shot and no repeat discharges were required.

Overall, the simulations are largely in agreement with the Stark broadening measurements of n_e. In the unseeded low-density discharge #27981, the modelling agrees with the measurements generally within a factor of 2, with good qualitative reproduction of the measured density distribution. The measured densities in the inner divertor are a factor of 10 higher than the upstream density, i.e. a high-density
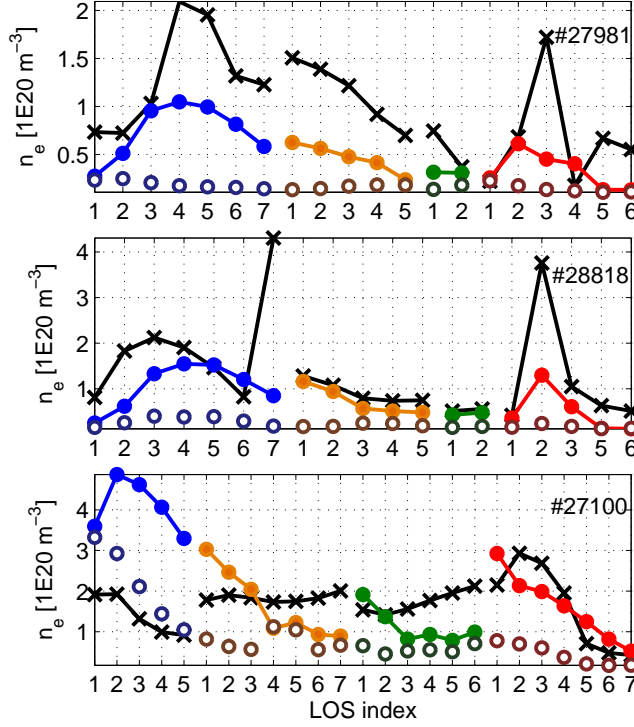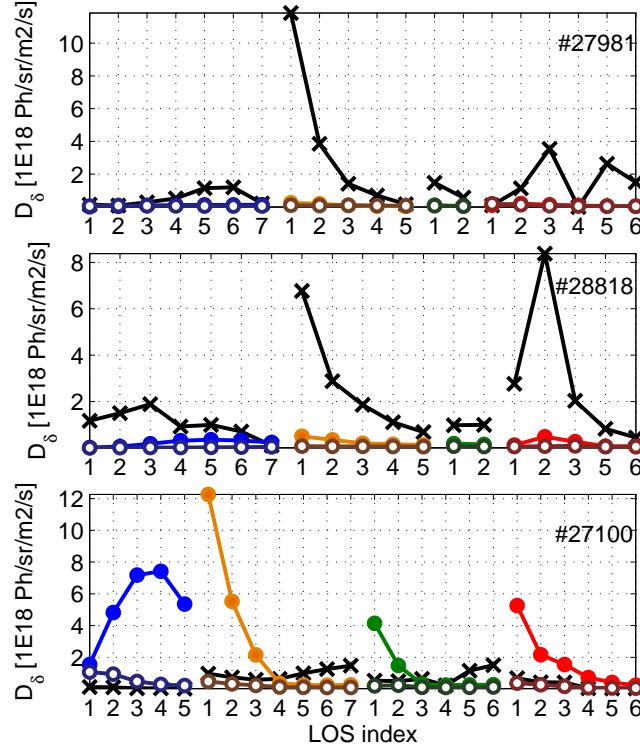
Figure 10. Comparisons between the modelled and measured electron densities, n_e, as calculated from the Stark broadening of the D_δ line along the LOS shown in Fig. 9. In #27100, a few more LOS were available with small differences in the alignment, see [24, 30]. The simulation results with drifts are drawn with the solid circles, and the colours correspond to the colours used in Fig. 9, indicating the LOS group. Within each LOS group, the indexing of the LOS goes from bottom to top, and from left to right. The corresponding experimental results are drawn with the black crosses, and the simulation results without drifts are drawn with the hollow circles. The results are shown for the following ASDEX Upgrade discharges: #27981 (cprresponding to the low-density reference discharge #27691, top row), #28818 (N-seeded low-density discharge, middle row), and #27100 (corresponding to the high-density discharge #27688, bottom row).

front, also known as the high-field-side high-density region (HFSHD) [31], exists near the target in both modelling and in the experiments. These observations are made only for the simulations with drifts. Without drifts, the agreement is significantly worse (more than a factor of 10 discrepancies), as no high-density front is created in the inner divertor in the simulations. In the N-seeded discharge #28818, the agreement along the blue LOS and along the horizontally distributed (green and yellow) LOS is even better than in the unseeded discharge, as the modelled densities are higher. In the high-density discharge, a similar agreement between the modelled and measured density within about a factor of 2 (or a factor of 3 for a few LOS) is obtained as in the unseeded low-density discharge, provided that the drifts are activated. Without drifts, the simulations yield too low densities for most of the LOS, but the differences with drift simulations are not as big as at low density.

Despite the good agreement with the n_e measurements, significant discrepancies

Figure 11. Comparisons between the modelled and measured D_δ emissions along the LOS shown in 9. The results are shown for the following ASDEX Upgrade discharges: #27691 (low-density reference discharge, top row), #28818 (N-seeded low-density discharge, middle row), and #27688 (high-density discharge, bottom row). Figure details as in Fig. 10.

are observed when comparing the modelled and the measured D_δ emission. In the low-density discharges #27981 and #28818 the D_δ emission is underestimated by the simulations along all sets of LOS, in line with the discrepancies observed with the low-resolution measurements discussed in Section 4.1. The discrepancies are largest along the yellow and red LOS (up to a factor of 50). In the high-density discharge #27100, the opposite observation is made: the simulations tend to overestimate the D_δ emission, particularly along those LOS which measure emission near the inner separatrix leg. Notably, the modelled emission in the high-density discharge #27100 corresponds closely to the measured emission in the low-density discharge #27981, particularly along the LOS for which the strongest discrepancies are observed (yellow and red). This suggests that the measured neutral conditions are reproduced in the modelling at a significantly (factor of 2) higher upstream density than what is used in the experiments.

These observations, in combination with the observations made in Sec. 4.1, suggest that there is a general problem with modelling the neutral emission and, therefore, the neutral densities in the two divertor legs of ASDEX Upgrade. Simultaneously, no obvious deficits were observed in the modelled plasma transport and the creation of a high-density front in the inner divertor in these L-mode
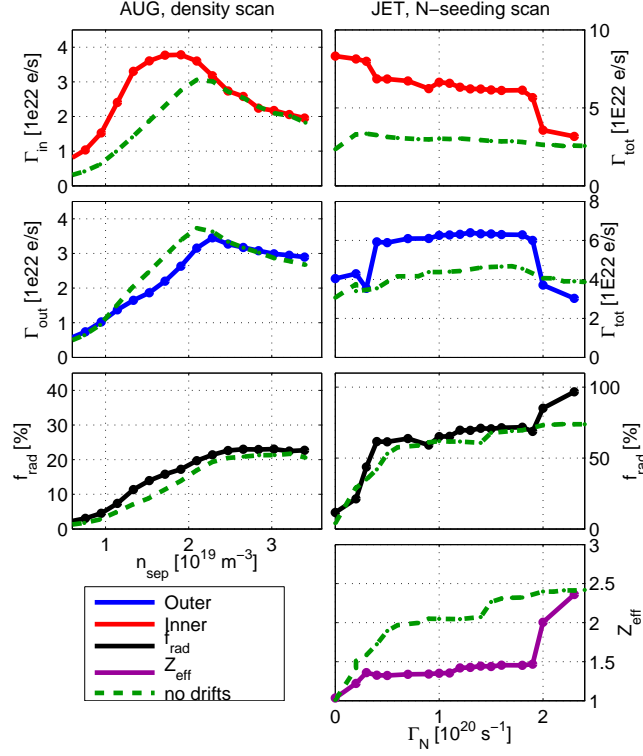
Figure 12. Top two rows: modelled ion fluxes to the two divertor targets as a function of upstream separatrix density (left) or impurity seeding rate (right). Bottom rows: modelled radiated power fraction (f_{rad}) and the effective charge (Z_{eff}) averaged over the simulated core flux surfaces at $\rho \sim 0.8-0.99$. The ASDEX Upgrade density scan (left) uses the input parameters selected for the low-density discharge #27691, and the JET impurity seeding scan (right) is based on the input parameters selected for the low-density discharge #82291. Only the upstream density (n_{sep}) or the impurity seeding rate (Γ_N) is varied between the various solutions for each device. The solid lines present the solutions obtained with all drift terms and currents activated, and the dashed lines give the corresponding solutions without drifts activated. The effective charge is shown only for the JET simulations with impurity seeding.

discharges. Possible reasons for the underestimation of the Balmer line emission, such as incorrect descriptions of the conductance and screening of neutrals in the modelling, are discussed further in Sec. 6.

5. The role of drifts

5.1. Observed effects of the drifts on divertor asymmetries and performance

The activation of drifts in the simulations was shown in the previous section to modify the solutions obtained with SOLPS5.0, for both ASDEX Upgrade and JET. Furthermore, the effects were observed to vary from one power exhaust regime to another. These observations are summarized in Fig. 12, which shows the evolution of the target ion fluxes ($\Gamma_{tot,in}$, $\Gamma_{tot,out}$) and the radiated power fractions (f_{rad}) with

increasing separatrix density (n_{sep}) in ASDEX Upgrade and with increasing nitrogen concentration (injected flux of N atoms, Γ_N) in JET. Both solutions without any activated drift terms but with currents activated (referred to as solutions *without drifts*) and solutions with fully activated drift terms and currents (referred to as solutions *with drifts*) are drawn with the dashed and solid lines, respectively. The ion fluxes and the radiated power fractions are used as figures of merit for characterizing the divertor asymmetries and performance. For simplicity, the input parameters, such as transport coefficients and recycling assumptions, are taken to be constant in each scan, corresponding to the low-density solutions in each device and with variations in n_{sep} or Γ_N only.

In the unseeded discharges, the largest effects of the drifts are observed at the inner target. At low–medium upstream densities, $n_{sep} \leq 2.4 \times 10^{19}$ m^{-3}, the drifts increase $\Gamma_{tot,in}$ and reduce $\Gamma_{tot,out}$. With drifts, the roll-over of $\Gamma_{tot,in}$ occurs at 20% lower upstream density compared to simulations without drifts. With drifts, the inner target detaches at 20% lower n_{sep} than the outer target, whereas without drifts, the roll-over is symmetric between the two targets. The drifts do not influence $\Gamma_{tot,in}$ or $\Gamma_{tot,out}$ in the detached regime at $n_{sep} > 2.4 \times 10^{19}$ m^{-3}, and also the radiated power fraction is similar both with drifts and without drifts. At the lowest densities, $n_{sep} < 1.2 \times 10^{19}$ m^{-3}, both $\Gamma_{tot,out}$ (corresponding to the low-recycling regime) and f_{rad} are unchanged by the drifts, but the drifts increase $\Gamma_{tot,in}$.

In the low-density seeded discharges, the drifts modify the solutions at all radiated power levels. This is seen in Fig. 12 in the seeding scan performed for JET, in which the evolution of the ion fluxes is drastically different depending on whether or not the drifts are activated in the calculations. In the low- and high-recycling regimes, corresponding to $\Gamma_N < 2 \times 10^{20}$ s^{-1}, the drifts increase the target ion fluxes by 50% (outer target) and 100% (inner target). In these regimes, with f_{rad} ranging between 15% and 70%, the total radiated power is nearly unchanged by the activation of drifts. However, Fig. 12 also shows the effective charge on the core flux surfaces, which is observed to increase from 1.3 to 2.2 at $f_{rad} = 60$ % in the simulations without drifts. This means that the drifts influence the spatial distribution of the radiation sources in the high-recycling regime (see also [21]). In the detached regime, the drifts do not influence the ion fluxes, but increase f_{rad} by $\sim 30\%$ compared to simulations without drifts.

5.2. Effect of drifts on the transport in the divertor

The drift effects observed in the divertor plasma stem from the modifications on the transport of power and particles caused by the drifts. As illustrated in Fig. 13, power and particles are transported into the divertor through the divertor entrance, which is located poloidally at the X-point height. The separatrix separates the entrance to the inner divertor from the entrance to the outer divertor. Below the X-point, transport between the two divertor legs can only occur through the PFR. In Fig. 14, we have analysed the outer divertor power and particle sources through each of these boundaries in various unseeded solutions. The solutions are shown with no drifts or currents activated, and with the $\mathbf{E} \times \mathbf{B}$ drifts, diamagnetic drifts and currents each individually activated. To ease the comparison between the different transport paths, the fluxes are normalized either to the total power or particle flux which arrives into the divertor from the upstream SOL (later referred to as *upstream power/particle flux*) or to the total power or particle flux at the targets (referred to as *target power/particle*
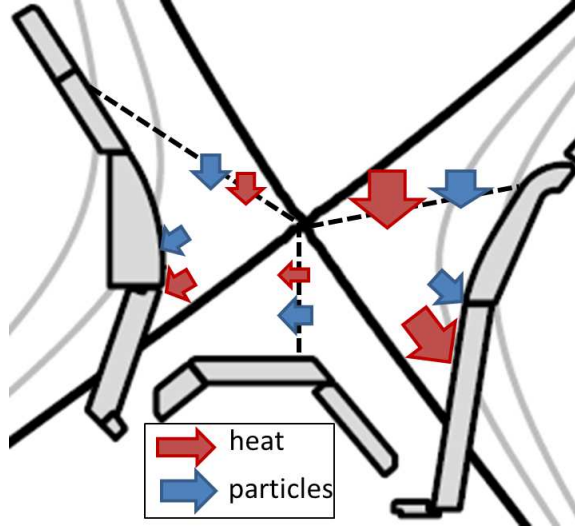
Figure 13. Illustration of the heat and particle flux channels which influence the divertor conditions. Heat and particles enter the two divertor legs from the upstream SOL at the X-point height. Inside the divertor, transport from one divertor into another can occur through the PFR below the X-point.

flux).

We analyse first the leftmost figure, which shows the asymmetry in the transport of particles and power from the upstream SOL into the two divertor legs. In the absence of drifts, the asymmetries arise from geometry and ballooning, which lead to a small majority of the upstream power flux being transported to the outer divertor instead of the inner divertor (60% of the upstream power flux goes to the outer divertor). The asymmetries in the particle fluxes vary with the density regime and device, and can be opposite to the power fluxes due to a strong parallel flow towards the inner divertor. The particle flux asymmetry is unchanged by the activation of all drift terms at high density ($n_{sep} = 2.2 \times 10^{19}$ m^{-3} in ASDEX Upgrade), and the change in the power flux asymmetry is small (70% of the upstream power flux goes to the outer divertor with drifts activated). At low density ($n_{sep} = 1.2 \times 10^{19}$ m^{-3} in ASDEX Upgrade or $n_{sep} = 1.5 \times 10^{19}$ m^{-3} in JET), however, the asymmetries particularly in the power fluxes are greatly enhanced by the activation of the $\mathbf{E} \times \mathbf{B}$ drifts. This results at low density in 90% of the upstream power flux to go to the outer divertor leg in both devices. The particle flux is much more symmetric in both devices.

The second particle and power flux channel to each divertor leg is through the private flux region, shown in the second column from the left in Fig. 14. In the PFR, the $\mathbf{E} \times \mathbf{B}$ drift transports both power and particles away from the outer divertor, towards the inner divertor, in both devices and both at high and low density. It is notable that the asymmetries in all the analysed particle and power flux channels are mostly affected by the activation of the $\mathbf{E} \times \mathbf{B}$ drifts. The asymmetries are little affected by the combination of currents and diamagnetic drifts alone.

Asymmetries in the particle and power fluxes at the divertor entrance do not necessarily lead to asymmetries in the divertor conditions, but merely in the circulation
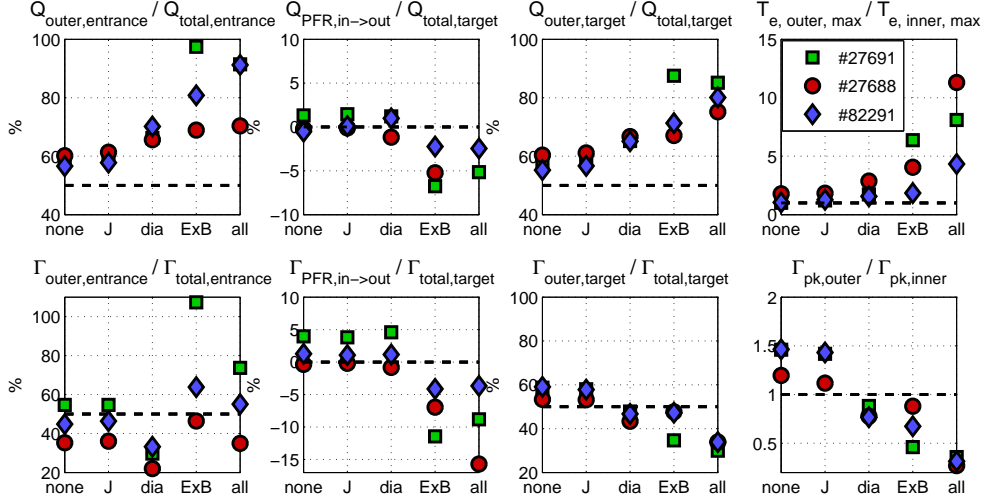
Figure 14. Calculated power fluxes (top row) and particle fluxes (bottom row) towards the outer target from the corresponding total fluxes towards the inner and outer targets. The fractions are calculated separately for the divertor entrance (left), the private flux region (middle left), and the divertor targets (middle right). The rightmost column shows the ratios of peak target temperatures (top) and peak ion fluxes (bottom) between the two targets. The modelling results are shown for discharges #27691 (AUG, low density, green squares), #27688 (AUG, high density, red circles), and #82291 (JET, low density, blue diamonds). The various physics models are activated in the simulations as follows: **none**: no drifts or currents; **J**: only currents activated; **dia**: diamagnetic drifts and currents activated; **ExB**: $E \times B$ drifts and currents activated; **all**: all drifts and currents activated. The horizontal dotted lines represent equal power sharing (taking into account the different toroidal lengths of the two targets) and symmetry of the peak quantities.

of particles and heat within the plasma. Inside the divertor legs, particles and heat can move through the separatrix between the SOL and the PFR due to the radial $E \times B$ drift and the anomalous transport. In the normal field configuration, the radial $E \times B$ drift is towards the PFR near the outer strike point and towards the SOL near the inner strike point, so that together with the poloidal $E \times B$ drift the particles may indeed circulate around the closed field-line region [22, 32]. However, the calculations show that with drift terms activated, the asymmetry in the power flux from the upstream SOL to the two divertor legs (90%) is stronger than the asymmetry in the corresponding particle flux (40–80%). In contrast, in the PFR, the $E \times B$ drift has a bigger influence on the particle transport (5–10%) than on the power transport (3–5%). In other words, the outer divertor receives in total more heat from the SOL and from the inner divertor than the inner divertor receives from the SOL and from the outer divertor, and this asymmetry in the net incoming heat flux is larger than the asymmetry in the net incoming particle flux. Therefore, the particles arriving to the outer divertor are hotter on average than those arriving to the inner divertor, which results in a lower plasma collisionality and a higher plasma temperature in the outer divertor leg, compared to the inner divertor leg. The lower collisionality leads to a higher heat conductivity in the outer divertor leg, which helps to maintain small parallel temperature gradients in the divertor volume and, consequently, a high target

temperature.

The role of the various convective and conductive heat flux components can be further examined in Fig. 15, which shows the various components of the poloidal heat flux in the low-density ASDEX Upgrade solution with and without drifts (bottom and top row, respectively). In the absence of drifts, the asymmetry in the upstream heat flux is largely due to the asymmetries in the conducted electron and ion heat flux, which account for 85% of the upstream heat flux. The rest of the heat flux is due to parallel flows. The contribution of currents to the upstream heat flux is small (0.05%) in the absence of drifts. However, as the $\mathbf{E} \times \mathbf{B}$ drift terms are activated, a significant increase in the convective heat fluxes is observed. The poloidal $\mathbf{E} \times \mathbf{B}$ drift in the main SOL is directly responsible for moving 5 % of the upstream heat flux away from the inner divertor and into the outer divertor. The contribution of currents is small in the present solution (0.5%), but it can be significantly larger if a different set of transport assumptions is used in the simulations [22] (significant currents have been observed particularly in H-mode studies, in which a transport barrier is introduced near the separatrix [18]). Furthermore, a significant increase is observed in the asymmetry of the conducted ion heat flux, reflecting the temperature asymmetry achieved already in the SOL above the divertor entrance by the activation of the $\mathbf{E} \times \mathbf{B}$ drifts.

In the PFR, the heat transport is almost entirely due to the poloidal $\mathbf{E} \times \mathbf{B}$ drift, which moves heat equivalent to 3 % of the upstream heat flux from the outer to the inner divertor leg, causing a small redistribution of power between the inner and the outer divertor below the X-point, in comparison to the asymmetry observed at the divertor entrance. The $\mathbf{E} \times \mathbf{B}$ driven particle flux in the PFR is equal to $\sim 70\%$ of the upstream particle flux. Because of the cool plasma temperatures in the PFR, the heat transport in the PFR plays a much smaller role in the overall heat circulation than what the corresponding $\mathbf{E} \times \mathbf{B}$ driven particle transport in the PFR plays in the overall particle circulation.

## 6. Discussion of remaining discrepancies – the role of neutrals

From the analysis presented in the previous sections, one can conclude that the drifts tend to bring the numerical divertor plasma solutions into a better agreement with the experimental data, as opposed to simulations performed without any activated drift terms. This is primarily due to the in/out asymmetries caused by the drifts, which are observed in present-day experiments particularly at low–medium densities. At high densities, when both divertors are at least in the high-recycling regime or even in the detached regime, the role of drifts in the divertor solutions reduces and the asymmetries become smaller. However, even when the target solutions show negligible effects of the drifts, the radiated power and its distribution may differ depending on whether the drifts are activated in the solutions or not.

Despite improving the agreement between the simulations and the measurements, the activation of drift terms does not bring the solutions to a perfect agreement with the experimental divertor conditions. Particularly, it is observed that in detached conditions in ASDEX Upgrade, the target ion fluxes are overestimated by SOLPS5.0 by up to a factor of 3. An over-estimation of the ion fluxes in detached conditions was observed also in previous studies for ASDEX Upgrade [2, 19] and JET [33]. An even more severe discrepancy is observed in the outer divertor in high-recycling conditions, in which the ion fluxes and neutral radiation are vastly (up to factors of 6 and 10, respectively) underestimated by the simulations, particularly at high
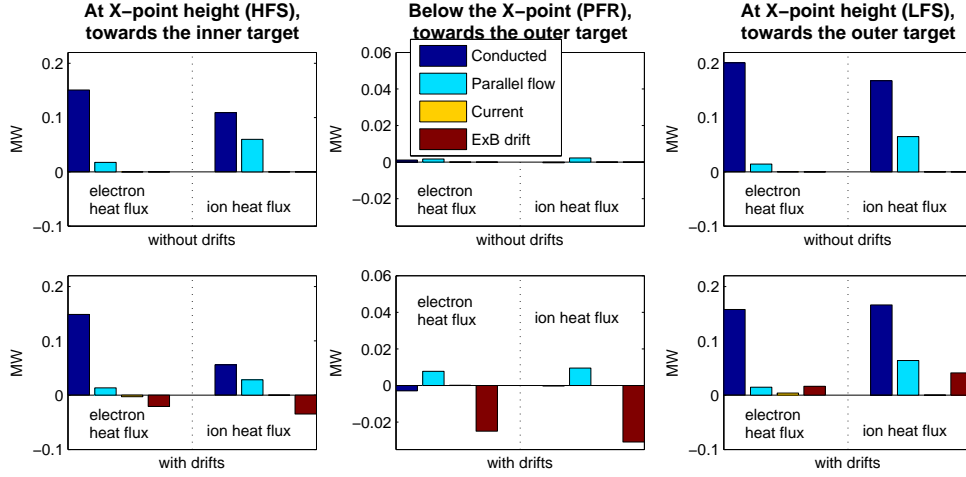
Figure 15. Calculated poloidal heat flux components for the low-density ASDEX Upgrade discharge #27691 at the divertor entrance and through the private flux region in the outer divertor. The results are obtained with activated $\mathbf{E} \times \mathbf{B}$ drifts and currents. The heat fluxes are calculated separately for the electron and ion channels. The positive direction is towards the inner target on the HFS, towards the outer target on the LFS, and towards the outer target in the private flux region.
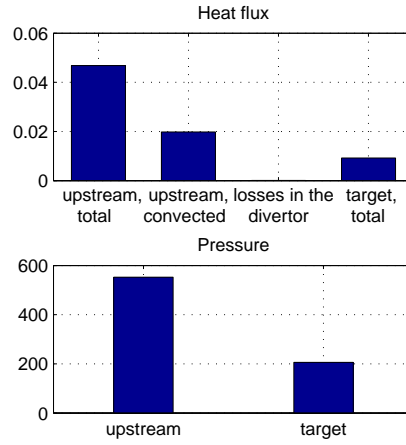
Figure 16. Calculated heat flux components and total pressure along the SOL flux tube which yields the highest outer target ion flux in the simulations for the high-density ASDEX Upgrade discharge #27688. Plotted are the total upstream heat flux, the convected fraction of the upstream heat flux, the energy losses due to radiation, CX, ionization and recombination, as well as the target heat flux. For the pressure only the total values upstream and at the target are plotted. The upstream location is taken to be at the divertor entrance.
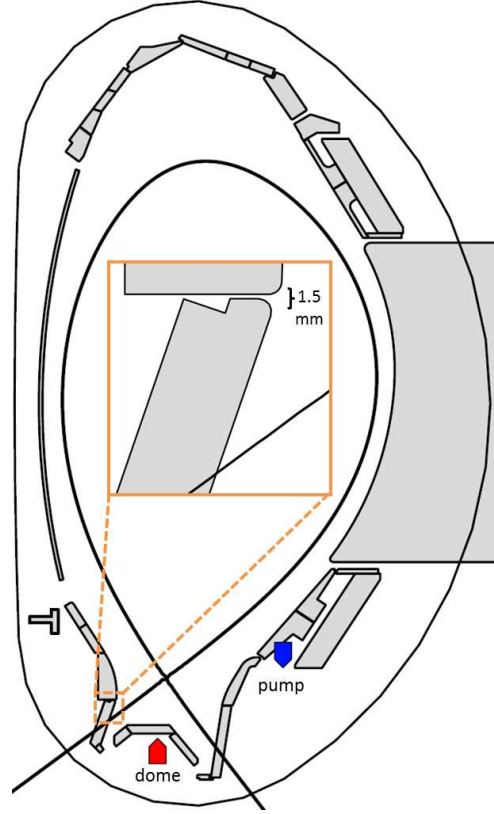
Figure 17. The ASDEX Upgrade vessel geometry and the locations of the dome and pump gauges. The inset shows a zoom-in of the inner target structure near the strike point location.

upstream densities. It is noteworthy that the discrepancies between the simulations and the experiments occur in those divertor regimes in which the experimental measurements deviate from the simple two-point model scaling, shown in Fig. 1 for ASDEX Upgrade. The underlying processes, which are not correctly accounted for in the simulations, could therefore be among those neglected in the simple two-point model scaling. These processes include volumetric power losses, momentum losses, as well as heat convection [34], all of which are included in the simulations, but perhaps with insufficient models for neutral–plasma interaction and transport.

A rough estimate of the role of the power and momentum losses, as well as of the convected energy fraction is obtained via the corrected two-point model [34]

$$\Gamma \propto \frac{f_{\mathrm{mom}}^2 f_{\mathrm{cond}}^{4/7}}{1 - f_{\mathrm{power}}}, \tag{1}$$

where f_{mom} describes the pressure loss between the upstream and target locations, f_{cond} is the conducted energy fraction, and f_{power} is the power loss fraction between the upstream and target locations (see [34] for details). Fig. 16 shows the modelled heat and pressure losses along the SOL flux tube in which the peak outer target ion fluxes are modelled at high n_{sep}. The figure shows that 50% of the upstream heat flux is carried by convection, and the heat flux is reduced to about 50% of the upstream value

Discharge	dome	pump	ratio
#27688	1.4E23 / 2.1E22 (1.2E22)	1.6E22 / 4.6E21 (2.5E21)	8.8 / 4.6 (4.8)
#27691	2E22 / 4.7E21 (4.3E21)	2.3E21 / 9.9E20 (9.2E20)	8.7 / 4.7 (4.7)

Table 2. The measured / modelled atomic flux densities ($1/m^2/s$) in the unseeded ASDEX Upgrade discharges (low and high density, bottom and top row, respectively) at the dome and pump gauge locations shown in Fig. 17. The last column shows the ratio between the flux densities at these two locations. The values shown in parentheses are from simulations which assume a neutral leakage path through the inner divertor structure, see Fig. 18.

at the target. Similarly, the pressure is reduced by 50% between the upstream and target locations. This yields an effective correction factor of 0.33. Hence, according to the modelling, the conditions should deviate from the 2-point model towards the opposite direction than what is seen in the experiments, Fig. 1. In other words, the simulations give a lower ion saturation current than the simple 2-point model, whereas in the experiments a higher ion saturation current is measured compared to the 2-point model.

It appears likely, that one or more of the simulated terms analysed above is in disagreement with the experiments. From Fig. 16 it is readily seen that the modelled losses associated with the plasma–neutral interactions in the high-recycling divertor conditions are small (instead, pressure and heat losses arise from radial transport). In Section 4.1, it was shown that in nearly all plasmas in the high-recycling or detached regimes, the modelled emission by the deuterium atoms deviates from the measured emission in the experiment, which could point towards an incorrect distribution of neutrals in the solution. More information about the neutrals is obtained from measurements by the neutral pressure gauges, several of which are located behind the divertor structures in ASDEX Upgrade. Table 2 compares the neutral flux measurements carried out under the dome and in the pumping region, see Fig. 17, with the modelled neutral fluxes at these locations. The neutral pressure is indeed underestimated by the simulations, and the largest discrepancies (a factor of 6) are observed when modelling the high-density discharge, in which also the discrepancies with the ion flux measurements are the largest, recall Fig. 8. The modelled relative fractions of neutrals between the two subdivertor regions are, however, largely (within a factor of 2) in an agreement with the measurements. This suggests that the conductance of neutrals in the subdivertor region is satisfactorily modelled, but the absolute number of neutrals is incorrect. This could either explain or be a consequence of the incorrectly modelled deuterium emission and, hence, incorrectly modelled power losses in the divertor. Because of this mismatch between the modelled and measured neutral densities, the modelled power and pressure losses associated with the charge exchange reactions are likely to be wrong too.

Possible explanations considered for the incorrect neutral description in the simulations include enhanced anomalous transport processes inside the divertor legs [14], as well as incorrectly modelled neutral transport paths due to details in the divertor and in the sub-divertor structures. The former were studied in [14], and here we briefly discuss the latter. Fig. 17 shows a typical gap between the divertor tiles, which cannot be accurately modelled with the SOLPS5.0 version. Although the poloidal width of the gap is only 1.5 mm, its location coincides with the location of the highest recycling source in the simulations, see Fig. 18. Consequently, the atomic flux
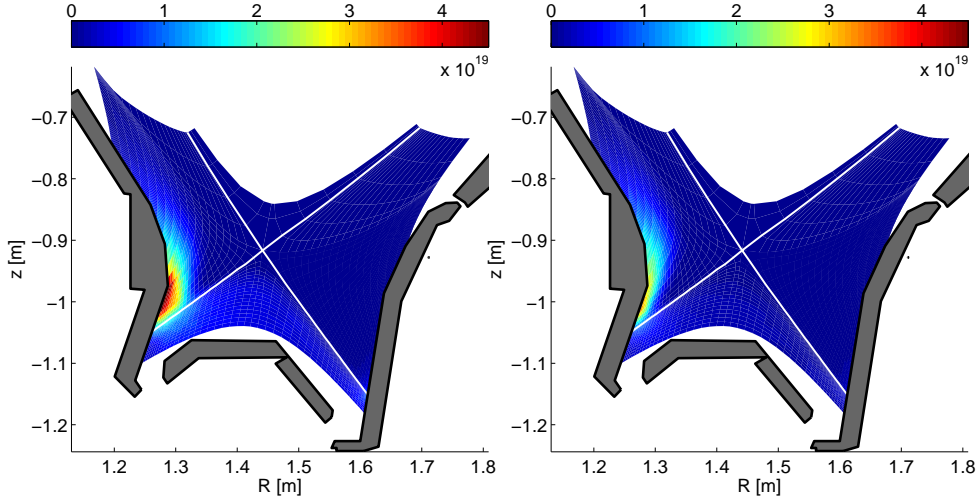
Figure 18. Modelled deuterium atomic densities ($1/m^3$) for the high-density ASDEX Upgrade discharge #27688. The figure on the left shows the results of the simulations with the default physics models (see Sec. 3). The figure on the right shows the results when 1% of the ions reaching the inner target are assumed to leak to the other (left) side of the inner target structure.

densities into the gap correspond to 1% of the total inner divertor recycling source. A simplified attempt to mimic the possible leakage through the inner divertor is made in Fig. 18 (right plot): Instead of full recycling at the inner target, we have assumed that 1% of all the ions arriving at the inner target are absorbed and a similar amount of neutrals is released by a gas puff on the other side of the target. The effect of this modification is readily seen in the distribution of deuterium atoms in the inner divertor. Before accounting for the leakage, the D atoms are largely concentrated near the gap between the two divertor tiles. After accounting for the leakage, the distribution of D atoms is broader along the target, as a significant fraction of fuelling occurs now through the PFR and the far SOL of the inner divertor. However, even with this modification the agreement with the pressure gauge measurements could not be improved, see the numbers in parentheses in Table 2. Therefore, the underlying reasons for the observed discrepancies remain unresolved. Nevertheless, as some modification of the divertor solutions is observed even with the simplified model of a single divertor gap, a proper inclusion of the various divertor leakage paths in a self-consistent manner could be an important future enhancement of the simulations and help bringing the neutral model closer to the experiments. For recent works addressing the effects of divertor leakage paths on the modelling of Alcator C-mod L-mode plasmas, see [35] (also [36, 37]). For the effects of poloidally varying transport coefficients on modelling the inner divertor of ASDEX Upgrade in H-mode, see [23].

7. Summary and conclusions

The present paper addressed the applicability of the plasma edge modelling tool SOLPS5.0 to model the divertor conditions in L-mode experiments in the two full-metal devices ASDEX Upgrade and JET. In particular, we addressed the effects

of the cross-field drifts and currents on the divertor solutions, and identified the improvements in view of matching the experimental signals obtained by the activation of the drift terms. It was shown that the divertor power and particle exhaust characteristics can be significantly asymmetric due to cross-field drifts, and the drifts affect the upstream density required for detachment (by 20% in ASDEX Upgrade) and modify the radiation pattern and the effective charge on closed field lines (50% reduction in JET). Furthermore, SOLPS5.0 simulations with drifts were shown to largely reproduce the measured temperature asymmetries in both ASDEX Upgrade and JET under conditions in which the outer divertor is in the low-recycling regime, as well as the measured ion flux asymmetries in JET at low density. Nevertheless, persisting discrepancies were observed at higher upstream densities. As concluded in earlier studies [24], the inner divertor of ASDEX Upgrade is in a detached regime already before the roll-over of the ion current, and under these conditions the measured target ion fluxes are overestimated by the simulations with drifts by up to a factor of 3, both with and without a significant N impurity concentration. Simultaneously, the density in the inner divertor volume can be matched within a factor of 2 over a wide range of upstream densities. A more significant discrepancy is, however, observed when the outer target enters the high-recycling regime and maximal ion fluxes are measured. In these conditions, the modelling underestimates the ion fluxes by up to a factor of 6. Simultaneously, the neutral Balmer line emission is underestimated by a factor of 10 and the sub-divertor neutral pressures are underestimated by a factor of 6. The various discrepancies appear to be connected to each other, but the ultimate cause of these deviations from the experiments is unclear. Part of the discrepancies might be explainable by the limited accuracy of the divertor structures and neutral transport paths in the simulations, but overall they do not seem to explain the large order of magnitude of the discrepancies between the measured and the modelled neutral densities and emission.

Acknowledgements

References

[1] Chankin A V *et al*, 2006 *Plasma Phys. Control. Fus.* **48** 839–868
[2] Wischmeier M *et al*, 2009 *J. Nucl. Mater.* **390-391** 250 – 254
[3] Kotov V *et al*, 2008 *Plasma Physics and Controlled Fusion* **50(10)** 105 012
[4] Aho-Mantila L *et al*, 2012 *Nuclear Fusion* **52(10)** 103 006
[5] Reimold F *et al*, 2015 *Journal of Nuclear Materials* **463** 128 – 134
[6] Schneider R *et al*, 2006 *Contrib. Plasma Phys.* **46(1-2)** 3–191
[7] Simonini R *et al*, 1994 *Contributions to Plasma Physics* **34(2-3)** 368–373
[8] Reiter D, 1992 *Journal of Nuclear Materials* **196** 80 – 89
[9] Wiesen S, 2006 *Edge2d/eirene code interface report.* Tech. rep., EFDA-JET
[10] Rognlien T D *et al*, 1994 *Contributions to Plasma Physics* **34(2-3)** 362–367
[11] Bufferand H *et al*, 2013 *Journal of Nuclear Materials* **438, Supplement** S445 – S448
[12] Shimizu K *et al*, 2009 *Nuclear Fusion* **49(6)** 065 028

[13] LaBombard B *et al*, 2004 *Nuclear Fusion* **44(10)** 1047
[14] Wischmeier M *et al*, 2012 In *Proc. 24th IAEA Fusion Energy Conf.*
[15] Pitts R *et al*, 2005 *Journal of Nuclear Materials* **337-339** 146 − 153
[16] Chankin A, 1997 *Journal of Nuclear Materials* **241-243** 199 − 213
[17] Rognlien T D *et al*, 1999 *Physics of Plasmas (1994-present)* **6(5)** 1851–1857
[18] Rozhansky V *et al*, 2012 *Nuclear Fusion* **52(10)** 103 017
[19] Wischmeier M *et al*, 2011 *Journal of Nuclear Materials* **415(1, Supplement)** S523 − S529
[20] Aho-Mantila L *et al*, 2014 In *Proc. 25th IAEA Fusion Energy Conf.*
[21] Aho-Mantila L *et al*, 2015 *Journal of Nuclear Materials* **463** 546 − 550
[22] Aho-Mantila L, Coster D and Wischmeier M, 2014 In *Proc. 41st EPS Conf. on Plasma Physics*
[23] Reimold F *et al*, 2016 *Nuclear Materials & Energy* **submitted to**
[24] Potzel S *et al*, 2014 *Nuclear Fusion* **54(1)** 013 001
[25] Aho-Mantila L *et al*, 2013 *Journal of Nuclear Materials* **438, Supplement(0)** S321 − S325
[26] Meisl G *et al*, 2015 *Journal of Nuclear Materials* **463** 668 − 671
[27] Meisl G *et al*, 2016 *Nuclear Fusion* **56(3)** 036 014
[28] Wiesen S *et al*, 2011 *Journal of Nuclear Materials* **415(1, Supplement)** S535 − S539
[29] Scarabosio A. *Private communication*
[30] Potzel S *et al*, 2014 *Plasma Physics and Controlled Fusion* **56(2)** 025 010
[31] Potzel S *et al*, 2015 *Journal of Nuclear Materials* **463** 541 − 545
[32] Chankin A V *et al*, 2015 *Plasma Physics and Controlled Fusion* **57(9)** 095 002
[33] Groth M *et al*, 2015 *Journal of Nuclear Materials* **463** 471 − 476
[34] Stangeby P, 2000 *The Plasma Boundary of Magnetic Fusion Devices.* IOP Publishing Ltd
[35] Dekeyser W *et al*, 2016 *Nuclear Materials & Energy* **submitted to**
[36] Lisgo S *et al*, 2005 *Journal of Nuclear Materials* **337339** 139 − 145
[37] Moulton D *et al*, 2015 In *Proc. 42nd EPS Conf. on Plasma Physics*